Characterization of Heterogeneous Regions in Polymer Systems Using Tapping Mode and Force Mode Atomic Force Microscopy

D. Raghavan,*,† M. VanLandingham,‡ X. Gu,† and T. Nguyen‡

Department of Chemistry, Polymer Science Division, Howard University, Washington, D.C. 20059, and Building and Fire Research Laboratory, National Institute of Standards and Technology, Gaithersburg, Maryland 20899

Received December 31, 1999. In Final Form: July 6, 2000

In this study, atomic force microscopy (AFM) is used to investigate the heterogeneity of blended films of poly(methyl methacrylate) (PMMA) and polybutadiene (PB) on silicon substrates before and after annealing. The blended films with different ratios of PMMA to PB are prepared by spin casting onto silicon substrates from solution. The surface morphology and composition of these cast films are investigated using tapping mode and force mode AFM. Annealing the samples in air at 75 ± 5 °C causes changes in the relative chemical and mechanical differences between PMMA and PB, so the phase image contrast is studied as a function of annealing time. The effect of tapping force level on phase image contrast is also explored. To identify the different components in polymer blends and to understand the influence of relative surface stiffness on the phase images, nanoscale indentation measurements are made on the observed phase-separated regions. Interpretation of AFM results is aided by data collected from both conditioned and annealed PB and PMMA films using Fourier transform infrared spectroscopy, dynamic mechanical analysis, differential scanning calorimetry, and contact angle measurements. A loss in phase contrast between PB-rich and PMMA-rich regions is observed as a function of heating time. This observation correlates well with the increases in glass transition temperature, modulus, and polarity of pure PB with respect to pure PMMA.

Introduction

Many polymer coatings are heterogeneous and contain degradation-susceptible regions, such as unreacted species and chemical additives.[1−4] These regions are suspected of being the sites for detrimental interactions between the external environment and the coating, as corrosion of the underlying substrate has been found to occur directly underneath these regions.[1−9] The sizes of these regions are believed to range from nanometers to micrometers. Therefore, mapping and identification of degradation-susceptible regions present on the surface of coatings are important scientific and technological challenges. Techniques that can discriminate and map the composition of these regions at the molecular level are therefore of fundamental interest. A wide range of techniques is available to map the heterogeneity in polymers, including spectroscopy and electron microscopy.[10−16] However, many of these techniques are only useful for studying size scales that are much larger than those of interest in this investigation.

Most of the investigations that have been performed on degradable regions of coating films have been limited to indirect techniques such as microhardness, dc resistance, ac impedance, and water uptake.[1−4] Progress in the characterization of degradable regions in coatings has been slow due to a lack of suitable analytical techniques.[17,18] One technique that has been used under ambient conditions to provide significant information about heterogeneity in polymers is atomic force microscopy (AFM).[19−25] AFM can provide spatial information along and perpendicular to the surface of the polymer film with resolution on the order of 1 nm.[26]

* To whom correspondence should be addressed. Telephone: (202) 806-4427. Fax (202) 806-5442. E-mail: draghavan@howard.edu.
† Howard University.
‡ NIST.

(1) Bascom, W. D. *J. Adhes.* **1970**, *2*, 168.
(2) Mayne, J. E. O.; Mills, D. J. *J. Oil Color Chem. Assoc.* **1975**, *58*, 155.
(3) Corti, H.; Fernandez-Prini, R.; Gomez D. *Prog. Org. Coat.* **1982**, *10*, 5.
(4) Mills, D. J.; Mayne, J. E. O. In *Corrosion Control by Organic Coatings*; Leidheiser, H., Ed.; National Association of Corrosion Engineers: Houston, TX, 1981; p 12.
(5) Wu, C. L.; Zhou, X. J.; Tan, Y. J. *Prog. Org. Coat.* **1995**, *25*, 379.
(6) Miskovic-Stankovic, V. B.; Drazic, D. M.; Teodorovic, M. J. *Corros. Sci.* **1995**, *37*, 241.
(7) Kinsella, E. M.; Mayne, J. E. O. *Br. Polym. J.* **1969**, *1*, 173.
(8) Mayne, J. E. O.; Scantleburg, S. *Br. Polym. J.* **1970**, *2*, 240.
(9) Fernandez-Prini, R.; Corti, H. *J. Coat. Technol.* **1977**, *49*, 62.
(10) Bierwagen, G. P.; Twite, R.; Chen, G.; Tallman, D. E. *Prog. Org. Coat.* **1997**, *32*, 25.
(11) Dunn, R. C.; Hotom, G. R.; Mets, L.; Xie, X. S. *J. Phys. Chem.* **1994**, *98*, 3094.
(12) Kumar, A.; Satija, S. K.; Han, C. C.; Slawecki, T. M.; Kumar, S. K.; Russell, T. P. *ACS PMSE Polym. Prepr.* **1994**, *71*, 280.
(13) Sung, L.; Douglas, J. F.; Han, C. C. *Phys. Rev. Lett.* **1996**, *76*, 4368.
(14) McEvoy, R.; Krause, S.; Wu, P. *Polymer* **1998**, *39*, 5223.
(15) Hasegawa, H.; Hashimoto, T. *Polymer* **1992**, *33*, 475.
(16) Winograd, N. *Anal. Chem.* **1993**, *65*, 622A.
(17) Nguyen, T.; Hubbard, J. B.; Pommersheim, J. M. *J. Coat. Technol.* **1996**, *68*, 45.
(18) Raghavan D.; Egwim, K. C. *J. Appl. Polym. Sci.* **2000**, *78*, 2454.
(19) Bar, G.; Thomann, Y.; Brandsch, R.; Cantow, H. J.; Whangbo, M. H. *Langmuir* **1997**, *13*, 3807.
(20) Bar, G.; Thomann, Y.; Brandsch, R.; Whangbo, M. H. *Langmuir* **1998**, *14*, 1219.
(21) Zhang, D.; Gracias, D. H.; Ward, R.; Gauckler, M.; Tian, Y.; Shen, Y. R.; Somarjai, G. A. *J. Phy. Chem. B* **1998**, *102*, 6225.
(22) McLean R. S.; Sauer, B. B. *Macromolecules* **1997**, *30*, 8314.
(23) Akhremitchev, B. B.; Mohney, B. K.; Marra, K. G.; Chapman, T. M.; Walker, G. C. *Langmuir* **1998**, *14*, 3976.
(24) Noy, A.; Vezenov, D.; Lieber, C. *Annu. Rev. Mater. Sci.* **1997**, *27*, 381.
(25) Noy, A.; Sanders, C. H.; Vezenov, D. V.; Wong, S. S.; Leiber, C. M. *Langmuir* **1998**, *14*, 1508.
(26) Leclere, P.; Lazzaroni, R.; Bredas, J. L.; Yu, J. M.; Dubois, P.; Jerome, R. *Langmuir* **1996**, *12*, 4317.

10.1021/la991694w CCC: $19.00
Published on Web 11/01/2000

The two most common modes of operation of AFM are contact mode and tapping mode. In contact mode, the tip is in constant contact with the surface of the sample, while in tapping mode the probe is oscillated such that the tip contacts the sample surface intermittently. This intermittent contact reduces tip−sample forces during imaging, resulting in minimal surface deformation of soft samples such as polymers and biological materials.[10,27−32] As the tip is brought into contact with the sample surface, changes occur in the probe oscillation, including phase angle, amplitude, and frequency, due to tip−sample interactions.[33] Often, a topographic image is produced by maintaining a constant amplitude, and a second image is recorded based on the changes in phase angle. This phase image or phase contrast image can often reveal heterogeneity in polymer samples.

While the phase changes of a probe oscillating in air have been related to energy dissipation between the tip and the sample surface, the relationships between the energy dissipation and the sample properties are not well understood.[34,35] In fact, from recent numerical modeling results, sample properties and characteristics such as the work of adhesion, local sample curvature, elastic modulus, and damping were all observed to affect the shape of dynamic force curves over nearly the entire range of tip−sample separation.[36] Attempts have been made to utilize contact models such as the Hertzian, Sneddon, and JKR models to qualitatively discuss changes in phase angle due to, in particular, the mechanical stiffness of the surface.[28] However, the complicated nature and dynamic aspects of tip−sample interactions during tapping mode render these types of models qualitative at best. Another numerical model was used to study various aspects of tapping mode AFM with respect to elastic and viscoelastic properties.[37] The material properties used as model inputs were elastic modulus and viscosity, with changes in adhesion force made by changing the Hamaker constant. While results of this model indicated that sources of possible phase contrast could include stiffness, damping, and hydrophilic/hydrophobic property variations, no relationships were derived relating phase changes to specific material properties. The only relationship between phase shift and sample properties found in the literature was given by Winkler et al., where phase shift was related to an effective frequency and an effective damping constant of the tip−sample system based on a number of simplifying assumptions to a numerical model.[38] The relationship of these frequency and damping parameters to sample properties, however, was not readily evident. Further, these authors state that the actual dependence of phase shift on material properties is highly nonlinear due to the combination of two surface potentials. Also, their approximate expression for phase shift is quantitative only for small damping constants and set points close to the free amplitude[38] and not for general imaging conditions.

Because of the difficulties in relating phase contrast to sample properties, the detailed assignment of features observed in phase images to the individual components of a heterogeneous sample requires careful study of the phase contrast under a variety of operational conditions.[39] For example, the level of force applied to the polymer surface can influence the image data, in particular the phase image data.[37,38,40] When both the level of applied force and the amplitude of free cantilever oscillation are large, the contrast of the phase image is often dominated by mechanical properties.[19] On the other hand, for lower force levels, competition between mechanical property differences and differences in tip−sample adhesion will affect the phase image contrast.[19] In general, the phase image data contains a wealth of information that can be useful for the characterization of multiphase and multicomponent polymer and coating systems, particularly when used in combination with other AFM modes and/or other analytical techniques.

To provide direct information on the local mechanical properties of various regions on the sample surface, the AFM can be used in force mode to measure the nanoscale indentation response of polymer surfaces.[41,42] Unlike tapping mode or contact mode, force mode is a nonimaging mode in which the probe tip is moved vertically with respect to the sample surface. Tip deflection is recorded as a function of the motion of the piezoelectric scanner in the *z*-direction producing a force curve. Force curves can be used to study the molecular attraction and repulsion between the tip and sample, including the mechanical properties of the localized regions.

In a previous paper, a combination of force mode and tapping mode AFM was used effectively to map mechanically heterogeneous regions in multicomponent polymer blends of polystyrene (PS) and polybutadiene (PB).[43] Good contrast was observed in the phase images of the blends between domain regions and the surrounding matrix in the unoxidized blend. Using force curves, the domains were shown to be rich in PS and the matrix to be rich in PB, as the tip penetration into the PB region was large while very little penetration occurred in the PS region. By controlled annealing of the polymer blend, the mechanical property difference between PS-rich regions and PB-rich regions was minimized. The increase in the relative stiffness of the PB matrix was evident using force curves, in which very little tip penetration was observed for either the domains or the matrix after annealing. This reduction of the stiffness difference corresponded to a large decrease in the phase image contrast between the PS-rich and PB-rich regions.

In this paper, a similar approach is used to map mechanically and chemically heterogeneous regions in multicomponent polymer blends of poly(methyl methacrylate) (PMMA) and polybutadiene (PB). This system was chosen because PMMA and PB differ significantly in both mechanical and chemical properties. However, by controlled annealing, both the chemical differences and

(27) Zhong, Q.; Innis, D.; Kjoller K.; Elings, V. B. *Surf. Sci.* **1993**, *290*, 1.
(28) Magonov, S. N.; Ellings, V.; Whangbo, M. H. *Surf. Sci.* **1997**, *375*, L385.
(29) Shao Z.; Yang, J. Q. *Rev. Biophys.* **1995**, *28*, 195.
(30) Umemura, K.; Arakawa, H.; Ikai, A. *Jpn. J. Appl. Phys., Part 1* **1993**, *2*, L1711.
(31) Radmacher, M.; Fritz, M.; Hansma, P. K. *Biophys. J.* **1995**, *69*, 264.
(32) Hansma, H. G.; Laney, D. E.; Bonilla, M.; Sinsheimer, R. L.; Hansma, P. K. *Biophys. J.* **1995**, *68*, 1672.
(33) Brandsh, R.; Bar, G.; Whangbo, M. H. *Langmuir* **1997**, *13*, 6349.
(34) Cleveland, J. P.; Anczykowski, B.; Schmid, A. E.; Elings, V. B. *Appl. Phys. Lett.* **1998**, *72*, 2613.
(35) Bar, G.; Brandsch, R.; Bruch, M.; Delineau, L.; Whangbo, M. H. *Surf. Sci.* **2000**, *444*, L11.
(36) Behrend, O. P.; Odoni, L.; Loubet, J. L.; Burnham, N. A. *Appl. Phys. Lett.* **1999**, *75*, 2551.
(37) Tamayo, J.; Garcia, R. *Langmuir* **1996**, *12*, 4430.
(38) Winkler, R. G.; Spatz, J. P.; Sheiko, S.; Moller, M.; Reinker, P.; Marti, O. *Phys. Rev. B* **1996**, *54*, 8908.
(39) Magonov, S. N. Personal communication, 1998.
(40) Spatz, J. P.; Sheiko, S.; Moller, M.; Winkler, R. G.; Reineker, P.; Marti, O. *Langmuir* **1997**, *13*, 4699.
(41) VanLandingham, M. R.; Dagastine, R. R.; Eduljee, R. F.; McCullough, R. L.; Gillespie, Jr., J. W. *Composites Part A* **1999**, *30*, 75.
(42) VanLandingham, M. R.; McKnight, S. H.; Palmese, G. R.; Elings, J. R.; Huang, X.; Bogetti, T. A.; Eduljee, R. F.; Gillespie, Jr., J. W. *J. Adhes.* **1997**, *64*, 31.
(43) Raghavan, D.; Gu, X.; Nguyen, T.; VanLandingham, M.; Karim, A. *Macromolecules* **2000**, *33*, 2573.

the mechanical differences of the bulk materials can be minimized. Thus, changes in the blend samples are studied as a function of annealing to investigate the effects of surface property differences on phase image contrast and force−distance curves. Results from contact angle measurements, Fourier transform infrared spectroscopy (FTIR), differential scanning calorimetry (DSC), and dynamic mechanical analysis (DMA) of bulk PMMA and PB samples are used to assist in the interpretation of the AFM results for the blends. The information generated can be useful in the mapping of degradation-susceptible regions in polymer coatings.

Experimental Section

Materials. Poly(methyl methacrylate) (PMMA) with a weight-average molecular weight, M_w, of 15 000 and polybutadiene (PB) with $M_w = 420\,000$ were acquired from the Aldrich Company. (Certain commercial instruments and materials are identified in this paper to adequately describe the experimental procedure. In no case does such identification imply recommendation or endorsement by the National Institute of Standards and Technology and Howard University, nor does it imply that the instruments or materials are necessarily the best available for the purpose.) The PB material contained cis, trans, and 1,2-addition components by mass fractions of 0.36, 0.55, and 0.09, respectively. Three blends were cast into thin films by a conventional solution cast method. Blend 1 had mass fractions of both PMMA and PB of 0.50 (hereafter designated as 50:50); blend 2 had a mass fraction of PMMA of 0.20 and a mass fraction of PB of 0.80 (hereafter designated 20:80); blend 3 had a mass fraction of PMMA of 0.80 and a mass fraction of PB of 0.20 (hereafter designated 80:20). These blends were prepared by mixing solutions of a mass fraction of PMMA of 0.02 in toluene and mass fraction of PB of 0.02 in toluene at the appropriate ratios and spin casting the solutions onto a precleaned silicon wafer at a speed of 2000 rpm for 30 s. Prior to application of the solutions, the silicon wafers were cleaned first with acetone and then with methanol, and then dried with a stream of nitrogen gas. All the cast films were conditioned for 24 h at 24 ± 2 °C under vacuum before analysis. (Throughout this text, each number following the symbol ± is the numerical value of an estimated standard deviation.) Some of the conditioned samples were analyzed without thermal treatment, while the other samples were heated in an air-vented oven at 75 ± 5 °C for up to 107 h. At specified time intervals, these samples were removed from the oven for investigation using AFM.

In addition to the blend samples, free-standing films of PB, cast films of PB, and cast films of PMMA were prepared so that changes in the PB-rich and PMMA-rich regions of the blend samples could be compared to the changes in the pure PB and PMMA films. The cast PB and PMMA films were prepared using a mass fraction of 0.02 of PB and PMMA, respectively, in toluene and the same spin-casting procedure described for the blend films. Free-standing PB films were made from a mass fraction of PB of 0.10 in toluene using a draw-down technique, in which the polymer solution was flooded on a release paper and a glass rod was firmly drawn across the paper to remove excess solution. Strips of masking tape were layered to the desired thickness and placed along the length of the release paper to control the film thickness. Free-standing PB and cast PMMA films were annealed at 75 ± 5 °C in an air-vented oven for up to 210 and 100 h, respectively. At specified time intervals, samples were removed from the oven for investigation of chemical and mechanical changes using contact angle measurements, FTIR, DSC, and DMA. Unfortunately, a free-standing thin film of PMMA of reasonable quality could not be obtained, and therefore no DMA measurements were made for PMMA.

Atomic Force Microscopy. Tapping mode AFM was used to characterize the polymer blend samples. A Dimension 3100 scanning probe microscope from Digital Instruments[1] was operated in tapping mode under ambient conditions (24 ± 2 °C, 45% RH ± 5% RH) using commercial silicon microcantilever probes. Manufacturer's values for the probe tip radius and probe spring constant are in the ranges of 5−10 nm and 20−100 N/m, respectively. Topographic and phase images were obtained simultaneously using a resonance frequency of approximately 300 kHz for the probe oscillation, a scan rate of 1 Hz, and a free-oscillation amplitude, A_0, of 60 ± 5 nm. For the majority of the investigations discussed in this paper, a set-point ratio, r_{sp}, of 0.80−0.90 was used, where r_{sp} is the ratio of the set-point amplitude (i.e., the constant amplitude maintained during imaging), A_{sp}, to A_0. For one study, however, r_{sp}, was varied from 0.84 down to 0.18 (i.e., from a light tapping force to a hard tapping force) to investigate the effect of tapping force level on the phase image contrast. Literature provides similar definitions to express the set-point ratio.[19,20,28,44]

To obtain mechanical responses of different domains in the blend films, nanoscale indentation was performed utilizing the same type of silicon cantilever described previously. For this application, force curves were obtained with the tip probing the regions of interest in the blend films. While more in-depth analysis of the force curves can be used to measure relative modulus values,[45,46] the identity of mechanically different regions can be inferred simply from the slope and shape of the repulsive or contact portion of the force curve. This technique was thus used to help identify the PB-rich and PMMA-rich regions of the samples.

AFM was also used to measure thicknesses of the cast films. For this application, a section of the film was removed with toluene to expose the silicon substrate. The average step height from the film surface to the surface of the substrate was used as an estimate of the film thickness. The result reported was the average of six measurements.

Contact Angle Measurements. To estimate the change in the polarity of PB-rich and PMMA-rich regions in the blends during annealing, contact angles of water (surface tension = 72.8 mJ/m^2 [47]) and methylene iodide (surface tension = 50.8 mJ/m^2 [47]) on PB and PMMA cast films were measured as a function of annealing time. A Rame-Hart goniometer was used to measure the advancing and receding angles of the liquids approximately 30 s after placing a drop on the sample surface. A minimum of six measurements was recorded for each liquid on each film. The average of these measurements was used to calculate the polar component of the surface free energy (γ^p), the total surface free energy (γ), and the polarity ($x^p = \gamma^p/\gamma$) for each film using the known surface tension values of the liquids and employing the geometric-mean approach of Owens and Wendt.[48]

FTIR Analysis. FTIR-transmission analysis of freshly prepared and annealed PB and PMMA cast films was used to determine the changes in PB-rich and PMMA-rich regions of the blend samples during annealing. FTIR transmission spectra of the cast PB and PMMA films were collected using a Nicolet 560x Fourier transform spectrometer equipped with a mercury−cadmium telluride (MCT) detector. All spectra were acquired as 200 signal-averaged scans with a resolution of 4 cm^{-1}. The transmission spectrum of the bare silicon substrate was used as the background. The integrated intensity of hydroxyl absorption in the range of 3300−3600 cm^{-1} and carbonyl absorption in the range of 1650−1850 cm^{-1} was used to determine oxidation in the cast films. Dry air was used as the purge gas.

DMA and DSC. DSC was used to measure the glass transition temperature, T_g, for fresh and annealed cast films of PMMA and annealed free-standing PB films, while the T_g of the fresh free-standing PB film was measured using DMA. DMA was also utilized to measure the room-temperature (24 °C) storage modulus, E', of fresh and annealed free-standing PB films. DSC was performed using a DSC 2910 (TA Instruments[1]) differential scanning calorimeter equipped with a refrigerated cooling system. Samples with masses ranging from 12 to 15 mg were sealed in

(44) Chen, X.; McGurk, S. L.; Davies, M. C.; Roberts, C. J.; Shakesheff, K. M.; Tendler, S. J. B.; Williams, P. M.; Davies, J.; Dawkes, A. C.; Domb, A. *Macromolecules* **1998**, *31*, 2278.

(45) VanLandingham, M. R.; McKnight, S. H.; Palmese, G. R.; Eduljee, R. F.; Gillespie, Jr., J. W.; McCullough, R. L. *J. Mater. Sci. Lett.* **1997**, *16*, 117.

(46) Howard, A. J.; Rye, R. R.; Houston, J. E. *J. Appl. Phys.* **1996**, *79*, 1885.

(47) Wu, S. *Polymer Interface and Adhesion*; Marcel Dekker: New York, 1982; p 151.

(48) Owens, D. K.; Wendt, R. C. *J. Appl. Polym. Sci.* **1969**, *13*, 1741.

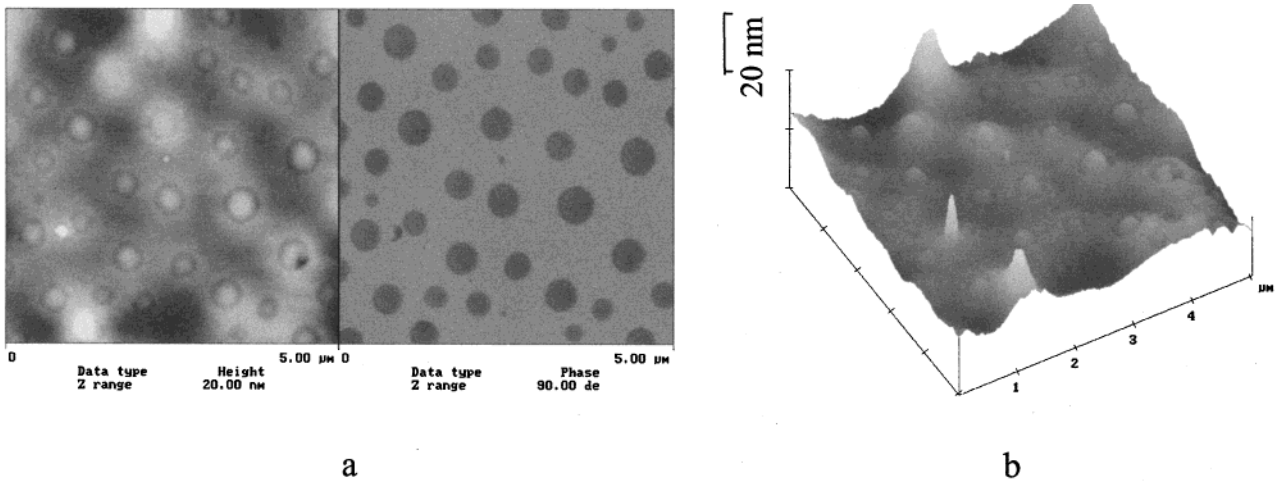

Figure 1. (a) Tapping mode AFM height image (left) and phase image (right); (b) a three-dimensional representation of the topography for the 20:80 blend after 24 h of ambient conditioning ($r_{sp} = 0.88$). Contrast variations are 20 nm from white to black for the height images and 90° from white to black for the phase image.

aluminum pans and subjected to a heating rate of 10 °C/min from −100 to 150 °C. DMA was carried out in a Rheometrics Solid Analyzer (RSA) II in the tensile mode at a frequency of 10 Hz and a dynamic strain of 0.05%. Films having dimensions of 12 mm by 35 mm and thicknesses that ranged from 0.05 to 0.09 mm were used. Experiments were conducted from −140 to 150 °C, and data were recorded in 2 °C increments.

Results and Discussion

AFM phase contrast can depend on a number of instrumental and noninstrumental parameters.[19,20,25,28,43,49,50] Instrumental parameters, which include the free oscillation amplitude (A_0), the set-point ratio (r_{sp}), and the operating environment, affect phase image contrast in a complex way. Depending on the interaction of these parameters, the contrast in a phase image can range from not observable to very large. For comparison of phase images of different samples or of the same sample over time, the same operational parameters were used during imaging, as outlined in the Experimental Section. Some of the noninstrumental factors that can affect phase image contrast include surface topography, the chemical nature and geometry of the tip, and the interactions between the AFM tip and different regions of the sample surface having different chemical and mechanical properties.[51−56] To understand the contribution of surface chemical and mechanical properties to phase image contrast, the PMMA/PB blend system was studied. The unannealed PMMA/PB blends represent samples with chemical and mechanical heterogeneity. The polarity of PMMA and of PB was determined to be 0.149 ± 0.021 and 0.009 ± 0.006, respectively, and the T_g values for the pure PMMA and PB films were measured to be 102 ± 2 °C and -102 ± 2 °C, respectively. Thus, PMMA represents a glassy polar material and unannealed PB is a rubbery and essentially nonpolar material. After controlled annealing in air for an extended period at elevated temperatures, the T_g, modulus, and polarity of PB are increased due to oxidation and cross-linking,[43] and the chemical and mechanical heterogeneity of the blend is reduced. First, the results of the studies of unannealed PMMA/PB blends are presented and discussed, followed by discussion of the effects of tapping force on the observed phase contrast, and finally discussion of the effects of annealing on the phase contrast.

Unannealed PMMA/PB Blends. In Figure 1a, AFM topographic (left) and phase (right) images are displayed for a spin-cast 20:80 blend film after 24 h of ambient conditioning ($r_{sp} = 0.88$). The thickness of this film was measured to be 375 ± 25 nm. In both the phase and topographic images, domains with a relatively circular cross section and a surrounding matrix are observed. This morphology is similar to patterns observed in other phase-segregated polymer blends.[19−21] A three-dimensional view of the topographic image is shown in Figure 1b. The average peak height for these domains is 5.0 ± 0.5 nm. Some of the domains are elevated (brighter in color), while a few domains are depressed (darker in color) with respect to the surrounding area. Unlike in the topographic image, however, all the domain structures have the same dark color in the phase image while the surrounding matrix is distinguished by a relatively uniform bright color. This observation indicates that the contrast observed in the phase image is not significantly influenced by topographic variations. From the phase image, the average diameter of the domains was found to be $0.42 \pm 0.05\ \mu$m, where the average is calculated using images of several different areas. The spacing of these domains was found to vary from area to area.

AFM images (topographic (left) and phase (right)) of the 50:50 and 80:20 blend films after 24 h of ambient conditioning are shown in Figures 2 and 3, respectively ($r_{sp} = 0.84$ for both sets of images). For comparison purposes, the thickness of the 50:50 blend was 250 ± 50 nm and that of the 80:20 blend was 180 ± 20 nm. Thus, the film thickness decreases as the mass fraction of PMMA increases. The phase images of these films again have noncontinuous domain structures of darker color surrounded by regions of brighter color similar to that of Figure 1a. For the 50:50 blend, however, large domains with a relatively circular cross section and a diameter of approximately $2.5 \pm 1.0\ \mu$m coexist with smaller domains

(49) Schmitz, I.; Schreiner, M.; Friedbacher, G.; Grasserbauer, M. *Appl. Surf. Sci.* **1997**, *115*, 190.
(50) Vezenov, D. V.; Noy, A.; Rozsnyai, L. F.; Lieber, C. M. *J. Am. Chem. Soc.* **1997**, *119*, 2006.
(51) Magonov, S. N.; Elings, V.; Papkov, V. S. *Polymer* **1997**, *38*, 297.
(52) Anczykowski, B.; Kruger, D.; Fuchs, H. *Phys. Rev. B* **1996**, *53*, 15485.
(53) Frisbe, C. D.; Rozsnyai, L. F.; Noy, A.; Wrighton, M. S.; Leiber, C. M. *Science* **1994**, *265*, 2071.
(54) Finot, M. O.; McDermott, M. T. *J. Am. Chem. Soc.* **1997**, *119*, 8564.
(55) Green, J.-B. D.; McDermott, M. T.; Porter, M. D. *J. Phys. Chem.* **1995**, *99*, 10960.
(56) Siinniah, S. K.; Steel, A. B.; Miller, C. J.; Reutt-Robey, J. E. *J. Am. Chem. Soc.* **1996**, *118*, 8925.

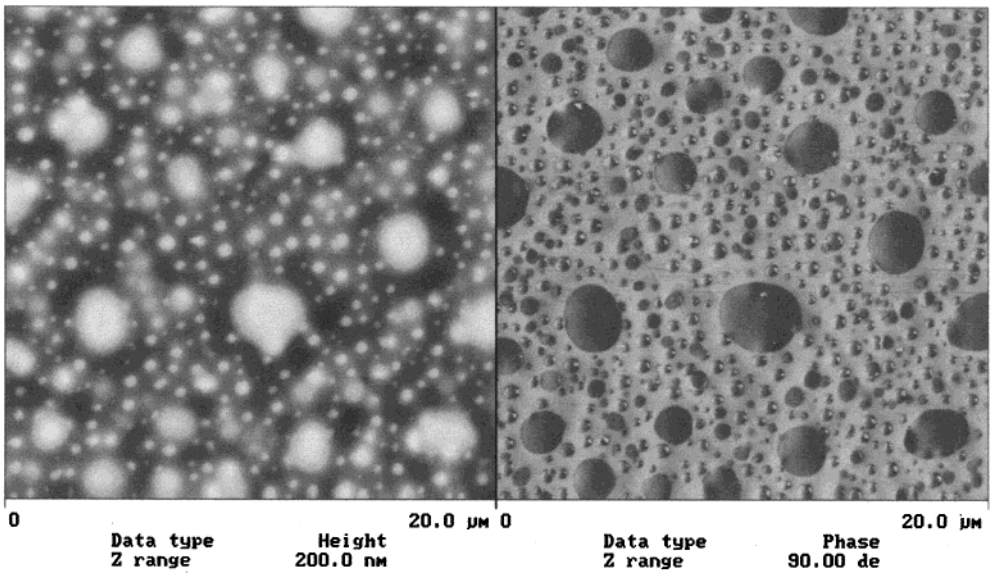

Figure 2. Tapping mode AFM height image (left) and phase image (right) for the 50:50 blend after 24 h of ambient conditioning ($r_{sp} = 0.84$). Contrast variations are 200 nm from white to black for the height image and 90° from white to black for the phase image.

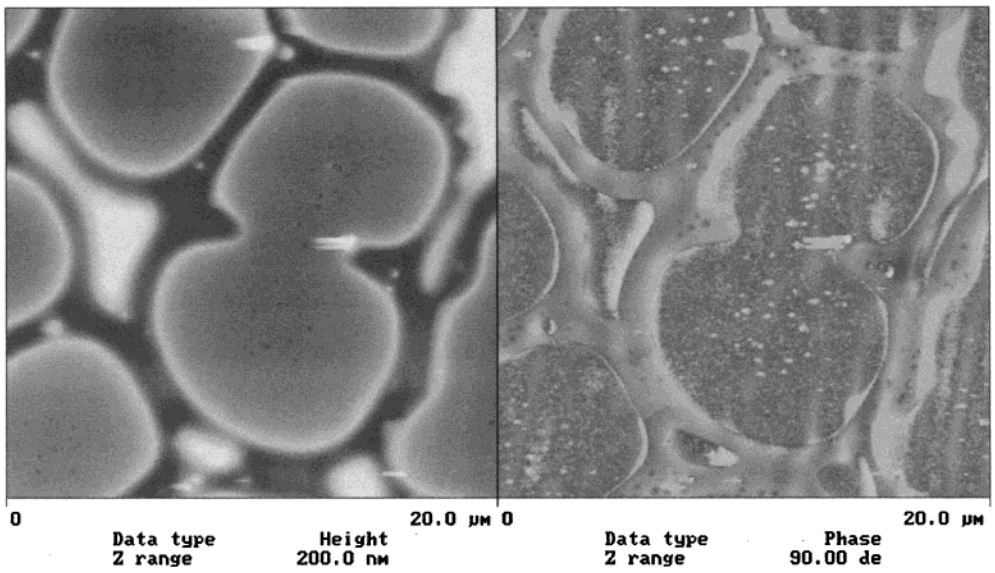

Figure 3. Tapping mode AFM height image (left) and phase image (right) for the 80:20 blend after 24 h of ambient conditioning ($r_{sp} = 0.84$). Contrast variations are 200 nm from white to black for the height image and 90° from white to black for the phase image.

that are 300−500 nm in size. Higher-resolution phase imaging (not shown) revealed that a majority of the small domains also have a relatively circular cross section. Further, the contrast of the small domains with respect to the surrounding matrix is similar to that of the large domains. For the 80:20 blend, the noncontinuous domains do not have circular cross sections in general, and the size of the domains is about 8 ± 2 μm. Thus, the average size of the domains increases with an increase in the mass fraction of PMMA in the PMMA/PB blends.

Upon close examination of the domains in Figure 3, a nanophase separation is observed within the domains, indicated by small "droplets" with bright contrast within the darker domains. The color of the droplets in the phase image appears to be similar to that of the surrounding matrix material. Similar observations have been made in other macromolecular blend systems.[20] This behavior is thought to be caused by hydrodynamic instability of the matrix component.[20,57−59]

To identify the domain and matrix regions as PB-rich and PMMA-rich or vice versa, the nanoscale indentation response of the different regions of each blend was studied using the AFM in force mode. In the force−distance curves for pure PMMA and pure PB films (not shown), tip penetration into the PB was significantly larger than that for the PMMA, which correlates to the lower stiffness of the PB compared to the glassy PMMA. Also, the larger tip penetration results in a larger contact area between the tip and the sample, which increases the adhesive pull-off force. Using the same tip and experimental conditions as used for the pure films, force−distance curves were measured for the domains and the surrounding matrix in each of the blends. The force curves for the dark phase domains and bright phase matrix of the 80:20 blend are

(57) Sung, L.; Karim, A.; Douglas, J. F.; Han, C. C. *Phys. Rev. Lett.* **1996**, *76*, 4368.
(58) Siggin, E. D. *Phys. Rev. A.* **1979**, *20*, 595.
(59) McMaster, L. P. *Adv. Chem. Ser.* **1975**, *142*, 43.

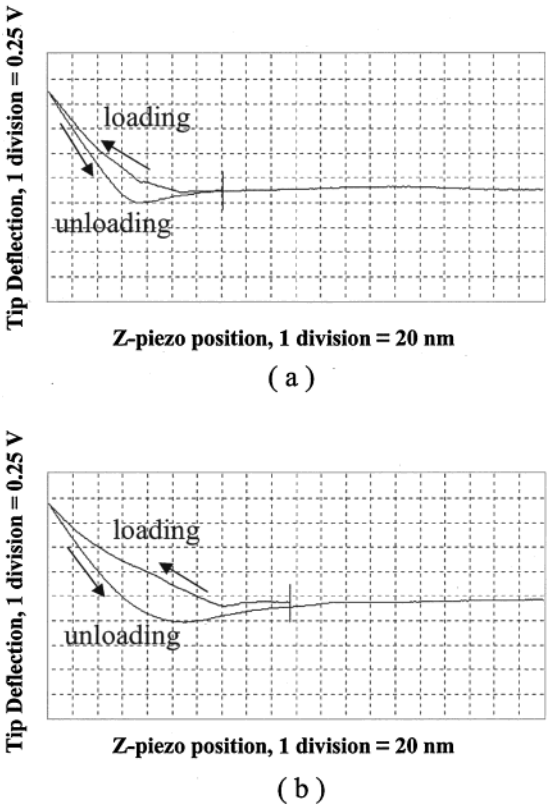

Figure 4. Typical force curves for (a) the domain region (darker color in the phase image) and (b) the matrix (brighter color in the phase image) for the 80:20 blend after 24 h of ambient conditioning.

shown in parts a and b, respectively, of Figure 4. A force curve can be divided into the repulsive region and the attractive region, where the repulsive region is characterized by positive tip deflection values and the attractive region is characterized by negative tip deflection values. Note that the horizontal portion of the force curve on the right half of both plots in Figure 4 corresponds to zero tip deflection, as the tip is well above the sample surface and no tip−sample interaction is occurring. The slope of the repulsive region for the dark domain (see Figure 4a) is steeper than that for the surrounding matrix (see Figure 4b) for both the extending and retracting curves. Further, for the dark domains, the reduction in tip deflection in the attractive region is less than that for the surrounding matrix such that the adhesive pull-off force is less. These observations indicate that the amount of tip penetration into the dark domain is less than that for the matrix. Further, the differences in the force curves for the domains and the matrix are similar to the differences between force curves for pure PMMA and pure PB discussed previously. Similar results were obtained for the 50:50 blend samples. However, the size of the domains of the 20:80 sample was similar to the size of the contact area during indentation, causing the measured response to represent not just the domain but also the surrounding matrix. Thus, only the compliant response of the matrix was measured for the 20:80 blend. Based on the indentation results for the 80:20 and 50:50 blends, the dark domains of the phase images in Figures 1−3 are likely to be PMMA-rich regions and the bright matrix surrounding the domains is rich in PB.

A more common method for identifying blend components is to perform image analysis using images of blends with different concentrations.[20,26] To compare this technique to identification using force curves, computer image analysis was used to measure the area fraction of the dark contrast regions for each of the blend samples. For these measurements, three 20 μm × 20 μm images of each film were analyzed. For the 20:80 blend, the area occupied by the domains is approximately 24% ± 3% of the scan area, while that for the 50:50 blend is approximately 39% ± 9% of the scan area and that for the 80:20 blend is approximately 69% ± 7% of the scan area. Although only a few small areas of each sample were analyzed, the area fraction of the darker domains seems to increase with increasing composition of PMMA in the blend. Thus, the identification of the domains as PMMA-rich regions using force curve analysis agrees with the image analysis results.

Effects of Tapping Force on Phase Image Contrast. With the successful identification of the domain and matrix regions in the PMMA/PB blends, the dependence of the phase contrast on the tapping force level was studied for a fixed free oscillation amplitude (A_0 = 60 ± 5 nm) using the 20:80 blend. In Figure 5a−f, topographic and phase images of the 20:80 blend are shown for r_{sp} = 0.84, 0.73, 0.58, 0.51, 0.40, and 0.18, respectively. Note that the sample used in this study was a different sample than that used for identification of the phase-separated regions and the probe tip was also different. These changes probably account for the slight differences (e.g., slight difference in domain sizes and slight difference in phase contrast between the domains and the matrix) that exist between Figure 1a and Figure 5a. As the tapping force level is increased (i.e., r_{sp} is decreased), the contrast changes in both the height images and the phase images in Figure 5. In fact, the contrast in the phase image flips (i.e., the lighter regions become the darker regions and vice versa) from r_{sp} = 0.84 to r_{sp} = 0.73 and then flips again from r_{sp} = 0.51 to r_{sp} = 0.40. Also, the topography of the domains relative to the matrix decreases by 6 ± 1 nm as r_{sp} is decreased from 0.84 to 0.58 and then increases by 15 ± 3 nm as r_{sp} is decreased from 0.58 to 0.18. These changes in phase and height are illustrated in Figures 6 and 7, respectively. Note that the changes in relative peak height were measured for only three domains, but the observed trends appear to be similar for all the domains in the imaged region.

In certain instances, anomalous height data can be produced due to deformation of the sample by the AFM probe tip.[19] In this case, the PB-rich matrix would be expected to deform more than the PMMA-rich domains as the tapping force is increased based on the previous discussion of force curves. However, the relative topography of the PMMA-rich domains decreases as r_{sp} is decreased from 0.84 to 0.58. Only for r_{sp} < 0.58 does the deformation of the PB-rich matrix cause an increase in the relative topography of the domains with increasing tapping force. For r_{sp} > 0.58, the changes in topography with force level are probably not a result of sample deformation. Rather, the decrease in the relative peak heights of the domains (see Figure 7) as r_{sp} decreases from 0.84 to 0.58 seems to correlate directly with the large increase in the relative phase value for the domains (see Figure 6b). Thus, the height changes as a function of force level for 0.84 ≥ r_{sp} ≥ 0.58 might be an artifact due to coupling between the phase data and the height data, while the height artifacts for r_{sp} < 0.58 are caused mainly by deformation of the PB-rich matrix.

Cleveland et al.[34] have recently shown that changes in a phase image are related to energy dissipation at the tip−sample junction. An increase in the attenuation of the probe oscillation that causes an increase in the phase lag could also cause a decrease in tapping amplitude possibly through a shift in the resonance frequency. The

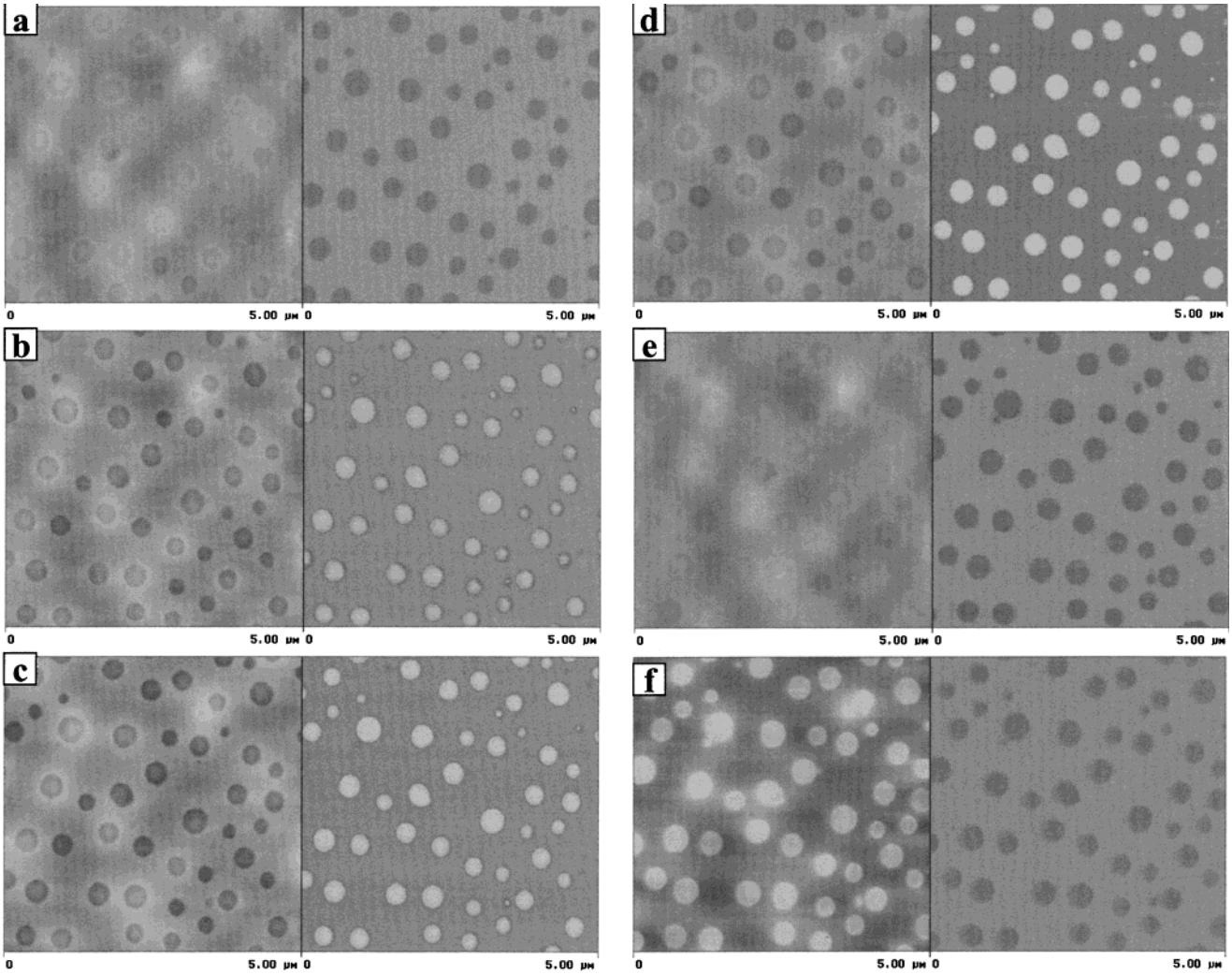

Figure 5. Tapping mode height images (left) and phase images (right) for a 20:80 blend sample after 24 h of ambient conditioning for various levels of tapping force: (a) $r_{sp} = 0.84$, (b) $r_{sp} = 0.73$, (c) $r_{sp} = 0.58$, (d) $r_{sp} = 0.51$, (e) $r_{sp} = 0.40$, and (f) $r_{sp} = 0.18$. Contrast variations are 30 nm from white to black for the height images and 90° from white to black for the phase image.

feedback mechanism of the AFM would react to such a change by increasing the tip−sample separation distance in order to restore the constant amplitude level. Thus, the regions with more phase lag (darker contrast) will appear higher in the topographic image than they actually are relative to the regions with less phase lag. This possible link between the phase lag and the tapping amplitude would explain the decrease in height of the PMMA-rich regions relative to the PB-rich matrix from $r_{sp} = 0.84$ to $r_{sp} = 0.58$. Regardless, a change in the phase contrast certainly appears to have an effect on the topographic data, which is an important consideration when analyzing AFM images.

Flipping of the phase contrast is often observed for r_{sp} values close to 1 (light tapping) due to the competition between attractive and repulsive tip−sample interaction forces.[34] As discussed previously, unannealed PB is essentially nonpolar while unannealed PMMA is highly polar. If the PB-rich and PMMA-rich regions in the blend have similar differences in polarity, differences in attractive interaction forces due to these polarity differences might significantly affect the phase contrast under light tapping conditions.[37] Thus, a change from attractive interaction to repulsive interaction might have caused the flip in phase contrast from $r_{sp} = 0.84$ to $r_{sp} = 0.73$. The flip in phase contrast from $r_{sp} = 0.51$ to $r_{sp} = 0.40$ is more difficult to explain. Bar et al.[20] also observed a similar second flip in phase contrast at a very low value of r_{sp}, postulating that the cantilever becomes trapped on the surface due to the contamination layer and thus the tapping mode becomes more like the force modulation mode. However, this explanation is unlikely in the present case, because the tapping mode amplitude is still approximately 30 nm when the second flip occurs (compared to 7.5 nm in the Bar et al. study), which is more than sufficient motion to escape the contamination layer. The second flip in the phase contrast might be related to the changes in topographic data. In the vicinity of $r_{sp} = 0.58$, the topographic data is affected by a competition between the increasing phase contrast and the increasing deformation of the PB-rich matrix. Perhaps as the matrix deformation becomes large with decreasing r_{sp}, the phase of the oscillating probe is changed significantly, causing the second flip in phase contrast. However, this second flip in phase contrast was not observed in a second study using the same sample but a different probe under similar operating conditions. Thus, perhaps the flip in phase contrast from $r_{sp} = 0.51$ to $r_{sp} = 0.40$ was due to a peculiarity with the particular probe under the given operating conditions. Further investigation of this phenomenon is required.

Effects of Annealing on Phase Contrast for PMMA/PB Blends. Exposing PB to elevated temperatures in air

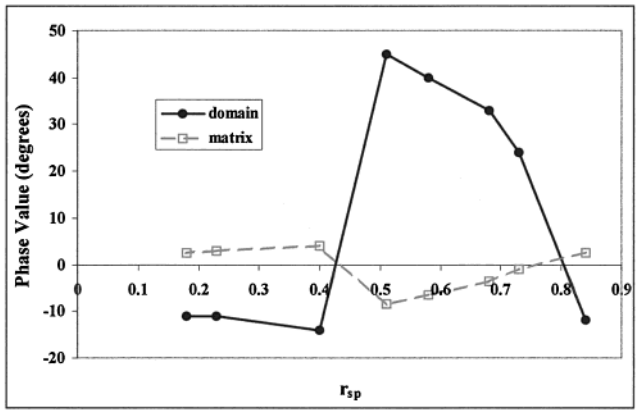

Figure 6. (a) Phase value as a function of r_{sp} for interactions between a silicon probe oscillating with $A_0 = 60 \pm 5$ nm and the domain and matrix regions of the 20:80 blend sample of Figure 5; (b) relative phase value (domain−matrix) as a function of r_{sp}.

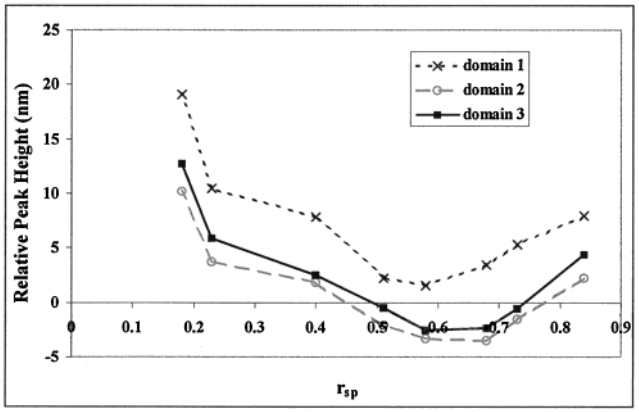

Figure 7. Relative domain height as a function of r_{sp} for three arbitrarily chosen domains of the 20:80 blend sample of Figure 5 (the observed trends appear to be similar for all the domains in the imaged region).

causes oxidation and cross-linking to occur.[60,61] As will be discussed, these changes cause increases in the polarity, modulus, and T_g of PB such that the chemical and mechanical property differences between PB and PMMA decrease with increasing annealing time. Assuming the changes in the pure films are similar to changes in the PMMA-rich and PB-rich regions of the blends, corresponding changes should occur in the AFM phase images and force curves.

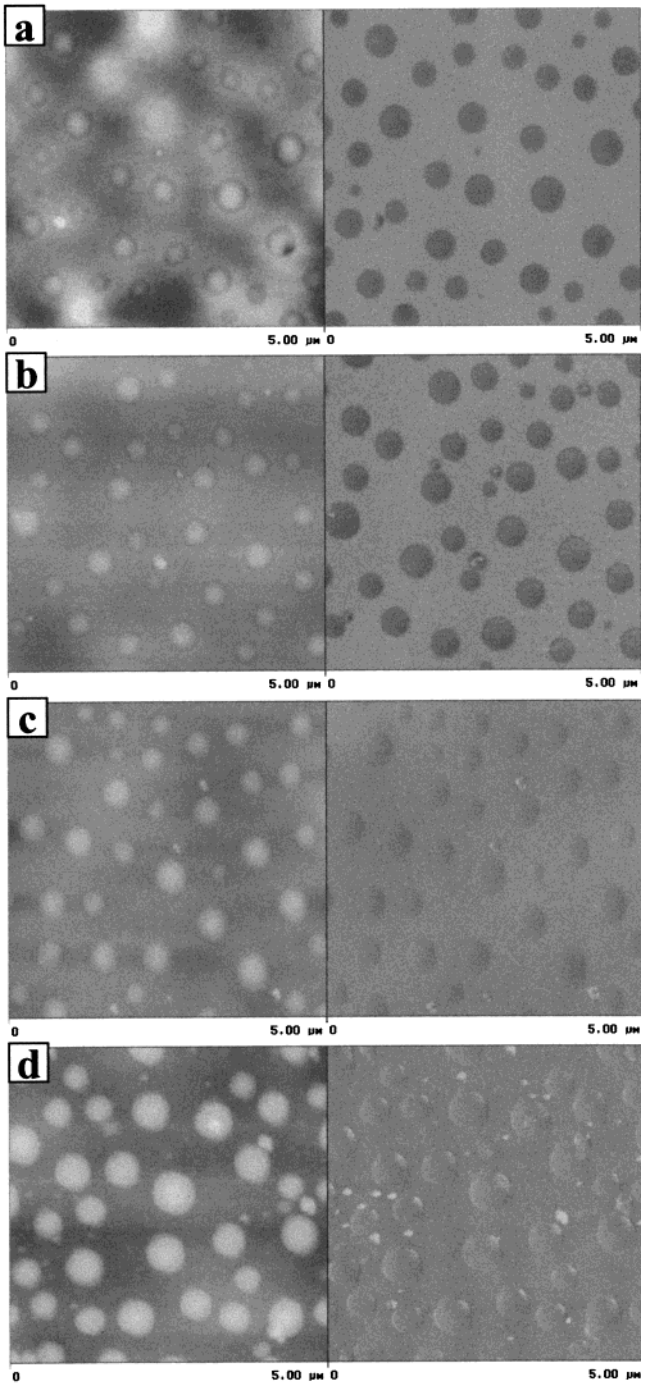

Figure 8. Tapping mode height images (left) and phase images (right) ($r_{sp} = 0.88$) for a 20:80 blend sample after 24 h of ambient conditioning and annealing at 75 ± 5 °C in air for (a) 0, (b) 5, (c) 20, and (d) 107 h. Contrast variations are 50 nm from white to black for the height images and 90° from white to black for the phase image.

In Figures 8a−d, topographic (left) and phase (right) images ($r_{sp} = 0.84$) of the 20:80 blend are shown for annealing times of 0, 5, 20, and 107 h, respectively, where the images shown in Figure 8a are the same as those in Figure 1a. The morphology of the blend, i.e., PMMA-rich domains with relatively circular cross sections in a PB-rich matrix, does not change with annealing. However, the phase contrast between the domain and matrix regions decreases with increasing annealing time. In fact, after 107 h of heating (see Figure 8d), the phase values of the

(60) Dikkie, R.; Carter III, R. O.; Hammond, J.; Parsons, J.; Holubka, J. W. *Ind. Eng. Chem. Prod. Res. Dev.* **1984**, *23*, 297.
(61) Beavan, F. W.; Philips, D. *Rubber Chem. Technol.* **1975**, *48*, 692.

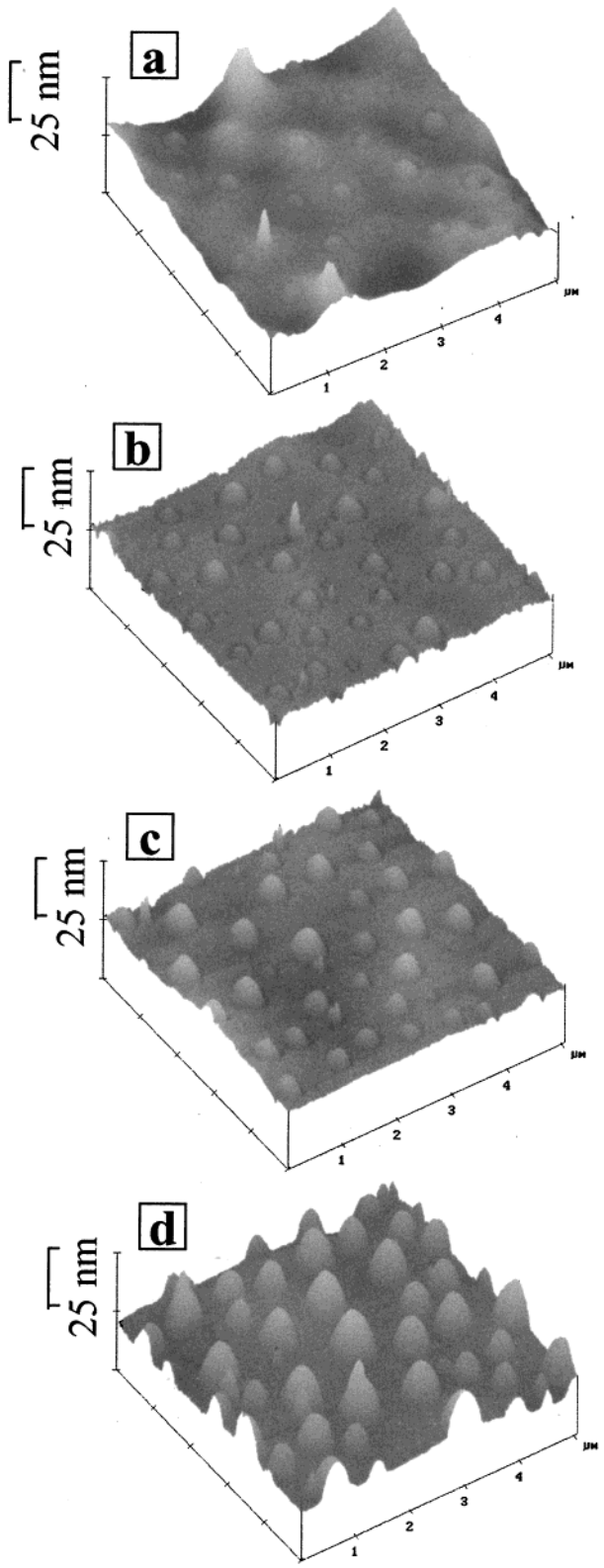

Figure 9. (a)−(d) Three-dimensional representations of the topographic images shown in Figure 5a−d, respectively.

domains and the matrix are approximately the same. Also, the heights of the PMMA-rich domains increase with respect to the PB-rich matrix with increasing annealing time. These height changes are depicted more clearly in the three-dimensional images shown in Figure 9, which correspond to the two-dimensional topographic images in Figure 8. Averaging over several domains, the average relative peak height was found to be 5 ± 1 nm, 5 ± 1 nm, 8 ± 2 nm, and 18 ± 3 nm for annealing times of 0, 5, 20, and 107 h, respectively. Recall that in comparing Figure 6b with Figure 7, the increase in the relative phase value of the domains (color becoming brighter) corresponded to a reduction in the relative heights of the domains due to a coupling between phase lag and the feedback amplitude. In Figure 8, however, the relative phase value for the domains increases with annealing time (color brightens to match that of the matrix), but the topography of the domains increases, not decreases, relative to the matrix. Therefore, the change in topography with annealing time is not a consequence of the changes in phase contrast. Most likely, the increase in the relative height of PMMA-rich domains is caused by shrinkage of the PB-rich matrix, because oxidation of the PB results in cross-linking, which in turn is often associated with polymer shrinkage. Similar changes in topography due to shrinkage of one of the components have been observed for other polymer blend systems after annealing.[62,63]

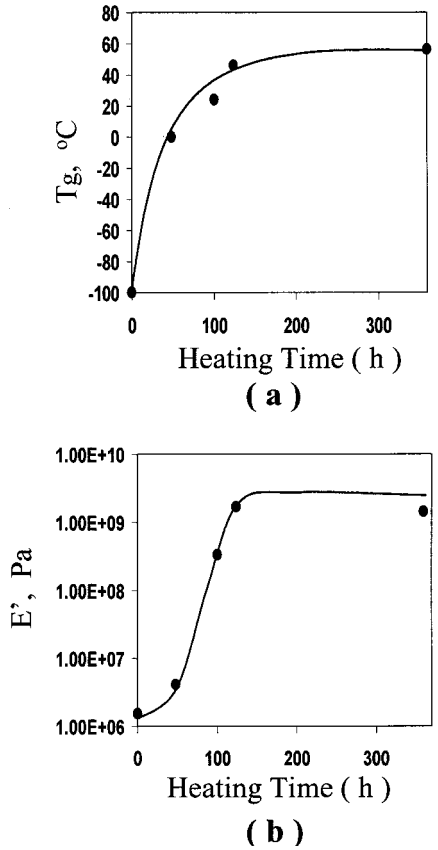

Figure 10. (a) T_g and (b) E' of a free-standing PB film as a function of heating time at 75 ± 5 °C in air.

To estimate the changes in mechanical properties of the PB-rich and PMMA-rich regions during annealing, DMA and DSC were used to measure changes in pure PB and PMMA films. The effects of annealing on the T_g and E' of PB are shown in Figure 10. The T_g of PB (measured using DSC) increases rapidly with heating time for the first 100 h before reaching a plateau at a value of approximately 56 °C. After the first 50 h of heating, E' for the PB film also increases rapidly as a function of annealing time before reaching a plateau at a value of approximately 1.5 GPa. The T_g of PMMA (measured using

(62) Motomatsu, M.; Mizutani, W.; Tokumoto, H. *Polymer* **1997**, *38* (8), 1779.
(63) Heck, B.; Arends, P.; Ganter, M.; Kressler, J.; Stuhn, B. *Macromolecules* **1997**, *30*, 4559.

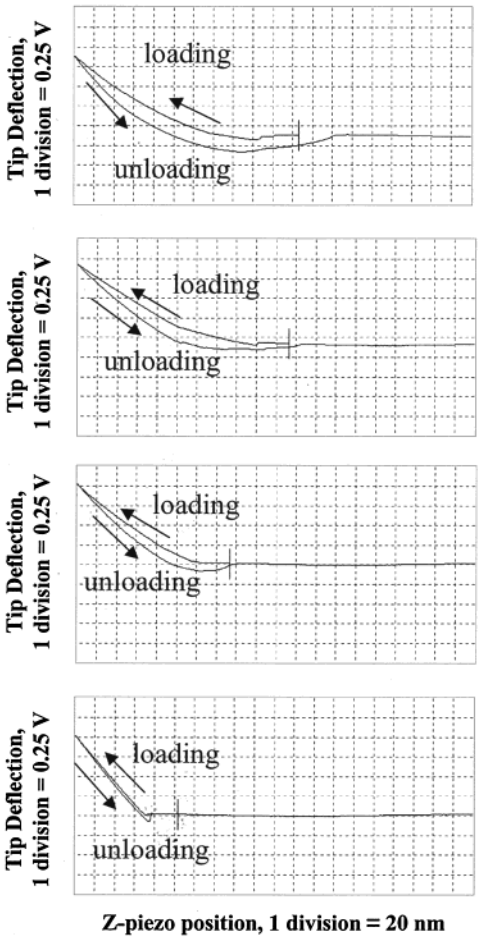

Figure 11. Force curves for the PB-rich matrix of a 20:80 blend sample after 24 h of ambient conditioning and (a) 0, (b) 5, (c) 20, and (d) 107 h of annealing.

DSC) before heating was 102 ± 2 °C and did not change significantly after annealing. The modulus of PMMA is expected to be approximately 3 GPa and should not be affected by annealing. Although the T_g and E' values of annealed PB after 100 h of heating are still lower than those of PMMA, the difference is much less than it was prior to annealing. Further, because the T_g of PB after 100 h of annealing is greater than the ambient temperature and the modulus has increased 3 orders of magnitude, the PB has changed from a soft, rubbery material to a glassy polymer. Thus, the PB-rich matrix in the 107 h annealed PMMA/PB blend samples should also exhibit glassy behavior.

To study the change in stiffness of the PB-rich matrix of the blends, force−distance measurements were made on the PB-rich and PMMA-rich regions of each PMMA/PB blend sample as a function of annealing time. Force−distance curves for the PB-rich matrix of the 20:80 blend are shown in Figure 11a−d for 0, 5, 20, and 107 h of heating, respectively. For comparison with the PMMA-rich domains, force curves corresponding to the domain and matrix regions from Figure 8d (the 20:80 blend after 107 h of heating) are shown in parts a and b, respectively, of Figure 12. Each of the curves shown in Figures 11 and 12 were taken using the same probe tip and similar operational settings. From the curves in Figure 11, the amount of tip penetration into the PB-rich region progressively decreases with increasing annealing time, as noted by the increase in the slope of the repulsive portion of the curve and the decrease in the tip−sample attraction. Further, as shown in Figure 12, the force curve of the

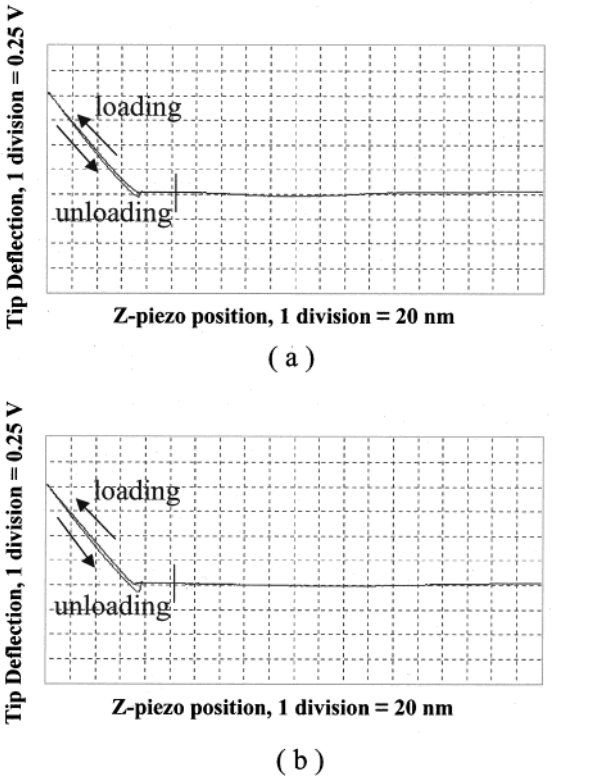

Figure 12. Force curves for (a) the PMMA-rich domain and (b) the PB-rich matrix for a 20:80 blend sample after 24 h of ambient conditioning and 107 h of annealing.

PB-rich matrix after 107 h of annealing is similar to that of the PMMA-rich domain. Note that the force curves taken on the PMMA-rich domain did not change appreciably with annealing time. The curves in Figure 12, however, mostly contain the bending response of the probe. In other words, no significant penetration of the tip into the sample occurs in either case because the stiffness of the probe is small compared to the stiffness of the samples. Therefore, the similarity in the force curves of Figure 12 does not imply similar modulus values, but from Figure 11, the stiffness of the PB-rich domains has certainly increased significantly with annealing and is probably approaching that of the PMMA-rich domains after annealing for 107 h.

To estimate the changes in chemical properties of the PB-rich and PMMA-rich regions during annealing, FTIR and contact angle measurements were used to measure changes in pure PB and pure PMMA films. For the FTIR studies, the formation of hydroxyl (OH) and carbonyl (C═O) groups was monitored as a function of heating time, the results of which are shown in Figure 13. In this figure, FTIR-transmission spectra are shown for wavenumbers of 1600−1900 cm^{-1} and 3250−3625 cm^{-1} for cast PB and PMMA films for several annealing times. For the PB film (see Figure 13a,b), the intensities for the C═O and OH groups, which are related to the extent of oxidation of the PB film, increase with annealing time up to approximately 100 h. For the PMMA film (see Figure 13c,d), no change in the intensity for the C═O and OH groups was observed. Assuming again that the behavior of the pure systems is similar to that of the phase-separated regions in the blends, the PB-rich regions of the blend films should be oxidized during annealing while the PMMA-rich regions should be thermally stable.

To determine the effect of annealing on the surface chemical properties, the polarity of freshly prepared and annealed PB and PMMA films was estimated using contact

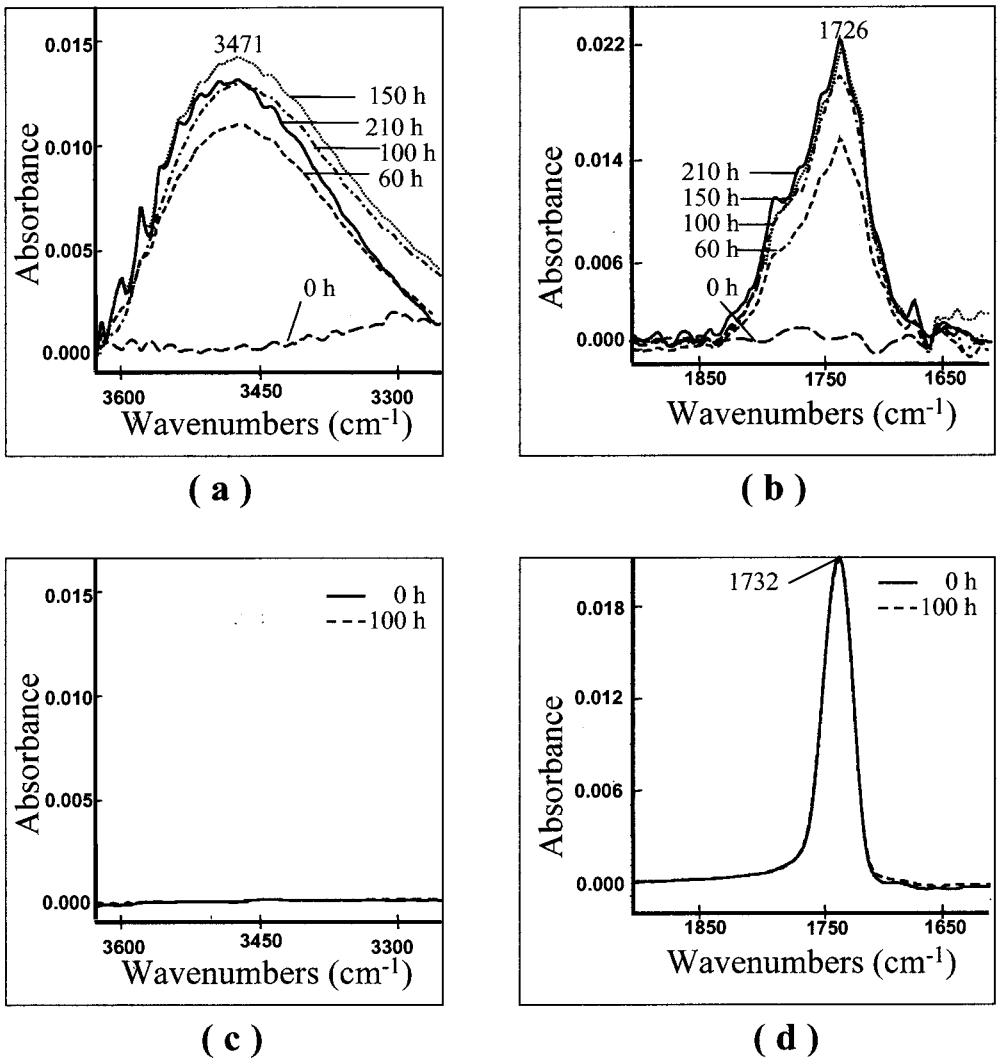

Figure 13. FTIR-transmission spectra in the (a) 3620−3250 cm^{-1} and (b) 1900−1600 cm^{-1} regions showing the effects of heating at 75 ± 5 °C in air on a cast PB film. Also shown in (c) and (d) are the corresponding spectra for a cast PMMA film, for which no changes in the spectra with heating time are observed.

Table 1. Contact Angles, Surface Free Energy Parameters, and Polarity of a Cast PB Film as a Function of Heating Time at 75 + 5 °C in Air[a]

	advancing contact angle (deg)					
heating time (h)	θ_w	θ_m	γ^d (mJ/m^2)	γ^p (mJ/m^2)	γ (mJ/m^2)	x^p
0	93 ± 2	36 ± 2	41.3 ± 0.4	0.40 ± 0.24	41.7 ± 0.2	0.009 ± 0.006
20	84 ± 1	36 ± 3	40.0 ± 1.1	2.18 ± 0.30	42.2 ± 1.0	0.046 ± 0.013
60	77 ± 1	36 ± 1	38.1 ± 0.6	5.35 ± 0.67	43.1 ± 0.3	0.124 ± 0.015
96	72 ± 2	35 ± 1	37.7 ± 0.3	6.89 ± 0.84	44.6 ± 0.6	0.154 ± 0.017
150	68 ± 1	36 ± 2	36.4 ± 1.0	9.37 ± 0.65	45.8 ± 0.8	0.205 ± 0.017
210	66 ± 1	38 ± 2	35.0 ± 1.0	10.75 ± 0.25	45.7 ± 1.2	0.237 ± 0.005

[a] θ_w, contact angle of water; θ_m, contact angle of methylene iodide; γ^d, nonpolar component; γ^p, polar component; γ, total surface free energy; x^p, polarity ($x^p = \gamma^p/\gamma$).

angle measurements with water and methylene iodide. The results for the PB film are shown in Table 1, while the results from PMMA are shown in Table 2. Annealing of PB in air caused an increase in the polarity from 0.009 ± 0.006 to 0.237 ± 0.005 after 210 h of heating in air. However, no significant changes in the polarity of PMMA were found after the same period of annealing. After 96 h of annealing, the polarity of PB (0.154 ± 0.017) was similar to that of PMMA (0.144 ± 0.019). Because these measurements are surface measurements, the similarity in the polarities of PB and PMMA after 96 h of annealing should correspond to similar polarities for the PB-rich regions and PMMA-rich regions in the blend samples after 107 h of annealing.

As presented previously, the phase image contrast of PMMA/PB blend films decreased with increasing annealing time (see Figure 8). In fact, after annealing for 107 h, the contrast between PMMA-rich domains and the PB-rich matrix is negligible, as shown in Figure 8d. The only remaining contrast in this figure is caused by the sensitivity of the phase of the oscillating probe to the topographic differences between the domain edges and the surrounding matrix, which has been enhanced due to the shrinkage of the matrix with annealing. Thus, after 107 h of annealing, the mechanical and chemical property differences between the domains and matrix have decreased while the topographic differences have increased,

Table 2. Contact Angles, Surface Free Energy Parameters, and Polarity of a Cast PMMA Film as a Function of Heating Time at 75 + 5 °C in Air[a]

	advancing contact angle (deg)					
heating time (h)	θ_w	θ_m	γ^d (mJ/m^2)	γ^p (mJ/m^2)	γ (mJ/m^2)	x^p
0	75 ± 2	39 ± 1	36.2 ± 0.6	6.37 ± 0.99	42.5 ± 0.8	0.149 ± 0.021
20	74 ± 1	39 ± 2	36.1 ± 0.8	6.64 ± 0.39	42.7 ± 0.7	0.155 ± 0.010
96	76 ± 1	41 ± 2	35.5 ± 1.2	5.95 ± 0.73	41.5 ± 0.4	0.144 ± 0.019

[a] θ_w, contact angle of water; θ_m, contact angle of methylene iodide; γ^d, nonpolar component; γ^p, polar component; γ, total surface free energy; x^p, polarity ($x^p = \gamma^p/\gamma$).

so that the only remaining phase contrast is due to the topography.

The contrast mechanisms in AFM phase images are complex. However, an understanding of the contrast variation due to chemical and mechanical heterogeneity in polymer systems can be obtained by systematic control of experimental variables. In this paper, the effect of set-point force level, polarity, and modulus on phase image contrast has been demonstrated. However, other factors can affect the contrast, including surface topography, the probe tip geometry, and the chemical nature of the tip.[35,64−67] Work is currently being conducted with chemically modified tips to obtain a better understanding of the tip−sample interactions in polymer blends, composites, and coatings.

Summary and Conclusions

Tapping mode and force mode AFM were used to examine the heterogeneity of blended films of PMMA and PB on silicon substrates. The surface morphology of three blends with different PMMA−PB compositions was determined based on a combination of phase contrast imaging and nanoscale indentation. The morphology of each blend consisted of PMMA-rich domains in a matrix of PB-rich material. The effect of tapping force level on phase image contrast was explored with one blend sample. Anomalous topographic changes were observed as a function of force level. For $0.84 \geq r_{sp} \geq 0.58$ (lighter tapping) the height artifacts were probably due to coupling between the phase data and the height data, while the height artifacts for $r_{sp} < 0.58$ (harder tapping) are caused mainly by deformation of the PB-rich matrix. Two contrast reversals were also observed in the phase images as the tapping force level was increased. The first flip was probably related to competition between attractive and repulsive tip−sample interaction forces, while the second flip at higher force levels might be related to the large deformation of the matrix region but could have been due to a peculiarity with the AFM probe. The effect of annealing on the blends samples was also studied as a function of heating time in air at 75 ± 5 °C. Large decreases in the phase image contrast between the domains and the matrix was observed with increasing annealing time. Also, the stiffness of the PB-rich matrix was found to increase with annealing time using nanoscale indentation. These phase contrast and stiffness changes corresponded well with changes in the relative chemical and mechanical differences between PMMA and PB, as measured using contact angle measurements, FTIR, DSC, and DMA. The thermal oxidation of PB caused increases in polarity, modulus, and T_g and also caused the PB-rich matrix to shrink, such that the relative heights of the domains increased with increasing annealing time.

Acknowledgment. This work was supported by the Air Force Office of Scientific Research under Grant F49620-98-1-0252.

LA991694W

(64) Vezenov, D. V.; Noy, A.; Rozsnyai, L. F.; Lieber, C. M. *J. Am. Chem. Soc.* **1997**, *119*, 2006.
(65) Eastman, T.; Zhu, D.-M. *Langmuir* **1996**, *12*, 2859.
(66) Binggeli, M.; Mate, C. M. *Appl. Phys. Lett.* **1994**, *65*, 415.
(67) Spatz, J. P.; Sheiko, S.; Moller, M.; Winkler, R. G.; Reineker, P.; Marti, O. *Nanotechnology* **1995**, *6*, 40.